Author Manuscript

Author Manuscript

Author Manuscript

Author Manuscript

HHS Public Access

Author manuscript

J Biomed Mater Res A. Author manuscript; available in PMC 2024 November 01.

Published in final edited form as:

J Biomed Mater Res A. 2023 November ; 111(11): 1768–1780. doi:10.1002/jbm.a.37587.

In vitro biological responses of plasma nanocoatings for coronary stent applications

ThiThuHa Phan[1], **John E. Jones**[2], **Meng Chen**[2,*], **T.L. Strawn**[4], **Hekmat B. Khoukaz**[4], **Yan Ji**[4], **Arun Kumar**[4], **Douglas K. Bowles**[3], **William P. Fay**[4], **Qingsong Yu**[1,*]

[1]Department of Mechanical and Aerospace Engineering, University of Missouri, Columbia, MO 65211

[2]Nanova, Inc., 1601 S Providence Rd, Columbia, MO 65211

[3]Department of Biomedical Sciences, University of Missouri, Columbia, MO 65211

[4]Department of Medicine, Division of Cardiovascular Medicine, School of Medicine, University of Missouri, Columbia, MO 65212

Abstract

In-stent restenosis and thrombosis remain to be long-term challenges in coronary stenting procedures. The objective of this study was to evaluate the *in vitro* biological responses of trimethylsilane (TMS) plasma nanocoatings modified with NH_3/O_2 (2:1 molar ratio) plasma post-treatment (TMS + NH_3/O_2 nanocoatings) on cobalt chromium (CoCr) alloy L605 coupons, L605 stents, and 316L stainless steel (SS) stents. Surface properties of the plasma nanocoatings with up to 2-year aging time were characterized by wettability assessment and X-ray photoelectron spectroscopy (XPS). It was found that TMS + NH_3/O_2 nanocoatings had a surface composition of 41.21 ± 1.06 at.% oxygen, 31.90 ± 1.08 at.% silicon, and 24.12 ± 1.7 at.% carbon, and very small but essential amount of 2.77 ± 0.18 at.% nitrogen. Surface chemical stability of the plasma coatings was noted with persistent O/Si atomic ratio of 1.292 – 1.413 and N/Si atomic ratio of ~0.087 through two years. The *in vitro* biological responses of plasma nanocoatings were studied by evaluating the cell proliferation and migration of porcine coronary artery endothelial cells (PCAECs) and smooth muscle cells (PCASMCs). 3-(4, 5-dimethylthiazol-2-yl)-2, 5-diphenyltetrazolium (MTT) assay results revealed that, after 7-day incubation, TMS + NH_3/O_2 nanocoatings maintained a similar level of PCAEC proliferation while showing a decrease in the viability of PCASMCs by 73 ± 19% as compared with uncoated L605 surfaces. Cell co-culture of PCAECs and PCASMCs results showed that, the cell ratio of PCAEC/PCASMC on TMS + NH_3/O_2 nanocoating surfaces was 1.5-fold higher than that on uncoated L605 surfaces, indicating enhanced selectivity for promoting PCAEC growth. Migration test showed comparable PCAEC migration distance for uncoated L605 and TMS + NH_3/O_2 nanocoatings. In contrast, PCASMC migration distance was reduced nearly 8.5-fold on TMS + NH_3/O_2 nanocoating surfaces as compared to the uncoated L605 surfaces. Platelet adhesion test using porcine whole blood showed lower adhered platelets distribution (by 70 ± 16%), reduced clotting attachment (by 54 ±12%), and

[*]Corresponding Authors: mengchen2002slc@yahoo.com, yuq@missouri.edu.

Conflicts of Interest: John Jones, Meng Chen and Qingsong Yu have financial interests in Nanova, Inc. The other authors declare no conflict of interest.

Author Manuscript Author Manuscript Author Manuscript Author Manuscript

less platelet activation on TMS + NH_3/O_2 nanocoating surfaces as compared with the uncoated L605 controls. It was further found that, under shear stress conditions of simulated blood flow, TMS + NH_3/O_2 nanocoating significantly inhibited platelet adhesion compared to the uncoated 316L SS stents and TMS nanocoated 316L SS stents. These results indicate that TMS + NH_3/O_2 nanocoatings are very promising in preventing both restenosis and thrombosis for coronary stent applications.

Keywords

Plasma nanocoatings; cell migration; platelet adhesion; restenosis and thrombosis prevention; coronary stent

1. Introduction

Coronary heart disease (CHD) remains a major cause of mortality in the US and worldwide [1-2]. Percutaneous coronary intervention (PCI) with stent implantation is an effective approach to treat occlusive CHD. Every year, almost 1.4 million stents are implanted globally [3]. Stent implantation causes endothelial denudation and inflammation, which promote vascular smooth muscle cell (SMC) proliferation and migration, resulting in restenosis [4,5-7]. Thrombosis, a potentially lethal complication of PCI [8-9], involves platelet adhesion and aggregation in conjunction with blood coagulation, triggered by exposure of subendothelial prothrombotic molecules to flowing blood [5,10]. Therefore, recovery of an intact endothelium is an important determinant of successful PCI [11]. The drug eluting stent (DES) has become the most used stent due to its capacity to release cytostatic drugs, such as everolimus, that inhibit SMC proliferation and in-stent restenosis. However, the remaining problem with DES is in-stent thrombosis, resulting from concomitant inhibition of endothelial cell proliferation and migration, delayed recovery of an intact endothelium, and consequently promoting activation of blood platelets and the clotting cascade by prothrombotic subendothelial molecules.

Stent thrombosis can occur acutely (within 24 hours), subacutely (between 1-30 days), late (from 1–12 months), or very late (beyond one year) after PCI. Late stent thrombosis (LST) and very late stent thrombosis (VLST), resulting from incomplete reendothelialization, inflammation, and acquired stent malapposition, occur significantly more frequently with sirolimus-eluting stents than bare metal stents [12-14]. Despite advances in stent design and drug delivery systems, LST and VLST persist as rare, but potentially life-threatening complications of DES. To combat stent thrombosis, patients are treated with dual antiplatelet therapy (DAPT) for extended periods after DES implantation, which increases bleeding risk, while also complicating the management of patients having surgical and other invasive procedures that require holding DAPT [15-17]. The newest generation DES have as short as 28–30-day indication for DAPT for patients with high bleeding risk. However, for most patients receiving a DES, 6–12-month DAPT is recommended. Therefore, there is a strong clinical need, especially for patients undergoing PCI in the absence of an acute coronary syndrome, to develop new stent technologies that prevent restenosis while having a low

Author Manuscript Author Manuscript Author Manuscript Author Manuscript

thrombosis risk, thereby reducing the need for prolonged DAPT and its associated risks, inconveniences, and cost [18-19].

Creation of bioactive stents that promote endothelial cell growth and migration, while inhibiting SMC proliferation and migration, is one such approach. Bioactive stent coatings containing nitrogen (N) and oxygen (O) functional groups may be a promising strategy to reduce restenosis and thrombosis after PCI [1,20]. Nitric oxide (NO), which is produced by vascular endothelial cells (ECs), accelerates vascular wall re-endothelialization, while inhibiting platelet activation, SMC proliferation, and inflammation [5,21]. In this study, gaseous mixtures of NH_3 and O_2 were used in conjunction with trimethylsilane [TMS, $(CH_3)_3$-SiH], an organosilicon compound containing a reactive Si-H bond, to produce plasma nanocoatings on cobalt chromium (CoCr) alloy L605 surfaces, including CoCr alloy L605 coronary stents. TMS plasma nanocoating remains firmly adhered to CoCr alloy L605 surfaces while covalently linking NO functionalities through NH_3/O_2 plasma post-treatment. The physical properties of nanocoated surfaces and stents were characterized, after which a series of experiments were performed to determine the effects of plasma nanocoating on platelet adhesion and aggregation, as well as the proliferation, migration, and viability of ECs and SMCs. The results of these experiments support the use of TMS + NH_3/O_2 nanocoated stents as a new approach to enhance endothelial recovery and combat restenosis and thrombosis after PCI.

2. Materials and methods

2.1. Sample preparation

Cobalt Chromium (CoCr) L605 alloy sheets (AMS 5537) purchased from HighTemp Metals (Sylmar, CA, USA) were sectioned into circular (diameter of 15 mm) and rectangular (15 mm × 30 mm) coupons. Rectangular coupons were bent to L-shape samples forming horizontal and vertical sections with identical surface areas. The L605 coupons were first cleaned in Detergent 8 solution (Alconox, Inc., White Plains, NY, USA) for 3 hours at room temperature in a tumbling jar, washed three times with deionized (DI) water by tumbling, and rinsed three times using acetone.

Stainless steel (SS) 316L stents (diameter × length = 1.6 mm × 12 mm) and CoCr L605 stents (diameter × length = 1.3 mm × 12 mm) were cleaned using the cleaning process recommended by the stent manufacturer (STI Laser Industries, Or Akiva, Israel). Stents were held in a sample rack immersed in a beaker containing ethanol for 15 minutes. The beaker containing stents was transferred to an ultrasonic bath filled with DI water held at 50°C and sonicated for 30 minutes. Each stent was rinsed with fresh ethanol using a squeeze bottle for 3 seconds. After cleaning, all samples (coupons and stents) were air dried and stored in clean glass Petri dishes before being used in this study.

Anhydrous ammonia (purity > 99.99 %) was purchased from Airgas Inc. (Holts Summit, MO, USA). Oxygen (purity > 99.6 %) was purchased from Praxair Inc. (Columbia, MO, USA). TMS (purity > 97 %) was purchased from Gelest, Inc. (Morrisville, PA, USA). A bell-jar reactor (80 L size) was used to generate direct current (DC) glow discharges. Samples were clipped to a titanium holder placed between two parallel titanium electrodes.

Author Manuscript Author Manuscript Author Manuscript Author Manuscript

The holder functioned as a cathode and the titanium electrodes served as electrically grounded anodes. The reactor was sealed and evacuated to a base pressure less than 1 mTorr using a series of mechanical and booster pumps. Gas flow rates were controlled with MKS mass flow controllers (MKS Instruments, Andover, MA, USA) and an MKS 247D Readout. The plasma reactor working pressure set point was 50 mTorr for all plasma processing steps using an MKS pressure controller. Plasma nanocoating preparation was performed in three main steps. First, oxygen plasma pre-treatment was conducted to remove potential organic contaminants on sample surfaces. Oxygen plasma treatment was performed for 2 min at an oxygen flow rate of 1 standard cubic centimeter per minute (sccm) and 20 W DC power. Second, after plasma pre-treatment, the reactor was pumped down to the base pressure and TMS was introduced to the reactor at a flow rate of 1 sccm. When TMS pressure stabilized at 50 mTorr, plasma nanocoating was initiated at 5 W DC power for 20 sec. Finally, TMS plasma nanocoatings were modified by plasma post-treatment using O_2 only (at flow rate 1 sccm), NH_3 only (at flow rate 1 sccm), and NH_3/O_2 mixture (at flow rate 2 sccm: 1 sccm). At the pressure of 50 mTorr, plasma was initiated and maintained at 5 W DC power for 2 min.

2.2. Surface characterization

Plasma nanocoating thickness was determined by using a microscope-mounted thin-film measurement device (Filmetrics F40-UV, KLA Corporation, Milpitas, CA, USA). The device is capable of measuring is 4 nm – 40 μm. A small sample area is non-destructively analyzed by reflecting light off the nanocoating. The reflectance spectrum was analyzed over a wavelength range (200-2000 nm). The Filmetrics software performs curve fitting of the reflectance spectrum to determine the nanocoating thickness.

Surface composition of the plasma nanocoatings was analyzed by X-ray photoelectron spectroscopy (XPS). A Kratos AXIS Ultra DLD X-ray Photoelectron Spectrometer (Kratos Analytical Inc., Chestnut Ridge, NY, USA) with a monochromatic Al Kα X-ray (1486.6 eV) source at 150 W was employed to examine coatings up to 10 nm depth. The X-ray source take-off angle was set at 90 degrees relative to the coupon surface, and the spot size was 200 μm in diameter. The survey scan was performed at 10 mA and 15 kV. Survey spectra were analyzed in the binding energy range of 1200 to −5 eV, and the time of 100 ms with two sweeps was used to resolve peaks. Samples were loaded into the load lock, pumped down to less than 5×10^{-7} Torr, and transferred into the sample analysis chamber. Data were collected at pressures approximately 5×10^{-9} Torr. Binding energies in survey and core-level spectra were calibrated with C 1s at 284.6 eV adventitious peak. The acquired data was interpreted by using the Casa XPS software. Peak fitting was carried out using Gaussian de-convolution function. The aged plasma nanocoated samples for XPS analysis were stored in Pyrex dishes at 25°C in cleaning room for up to 96 weeks to assess nanocoating stability to aging.

2.3. Cell culture of porcine coronary artery endothelial cells (PCAECs) and smooth muscle cells (PCASMCs)

Porcine coronary artery endothelial cells (PCAECs) and smooth muscle cells (PCASMCs), which were prepared as described [22], were re-suspended and cultured in Dulbecco's modified eagle medium (DMEM) (1X) and DMEM/F12 growth media, respectively, which

Author Manuscript Author Manuscript Author Manuscript Author Manuscript

were supplemented with 10% fetal bovine serum (FBS), penicillin/streptomycin (P/S), and L-glutamine [23]. The cells were grown in T-75 flasks in 15 mL of growth medium. Cells were grown from passage 7 to 8 in a humidified atmosphere with 5% CO_2 at 37°C. Culture media were replaced every 2 days for both PCASMCs and PCAECs until the cells reached 70% confluence. Cells were detached from the culture flasks with 0.25 wt.% trypsin-ethylenediaminetetraacetic acid (EDTA) (Sigma-Aldrich, St. Louis, MO, USA) and counted with a hemocytometer. At a concentration of 10,000 cells/mL, PCAECs or PCASMCs were seeded onto 15-mm-diameter coupons of uncoated L605, coupons with TMS plasma nanocoating, and coupons with NH_3/O_2 post-treated TMS plasma nanocoatings, placed in each well of 24-well cell plates, and cultured for up to 7 days. The coupons were UV-sterilized for 15 min per side prior to cell culture.

2.4. Cell proliferation and viability

Cell proliferation was evaluated by microscopic observation and quantified with the 3-(4, 5-dimethylthiazol-2-yl)-2, 5-diphenyltetrazolium (MTT) assay, which measures viable, metabolically active cells [4-5,16,19]. Following time points of 1-, 3-, and 7-day cell culture, the seeded coupons were incubated in MTT solution (0.5 mg/mL, 37 °C, 5% CO_2) for 4 h. Following incubation, the growth medium was removed from wells, dimethyl sulfoxide (DMSO) was added to solubilize formazan, and the optical absorbance at the wavelength of 570 nm was measured using a micro plate reader.

2.5. Cell morphologies

Porcine coronary artery endothelial cells (PCAECs) and smooth muscle cells (PCASMCs) were seeded on uncoated L605 and plasma nanocoated coupons. Each cell type was grown for 1, 3, and 7 days. For each time point, cells were rinsed once with phosphate-buffered saline (PBS) and fixed with sodium cacodylate (2% glutaraldehyde and 2% paraformaldehyde) for 30 min at room temperature. Cells were dehydrated in a graded series of ethanol (50%, 60%, 70%, 80%, 90% and 100%) incubations (10 min each) and dried in ambient air. The cell attachment and morphologies were examined by an FEI Quanta 600 FEG Environmental scanning electron microscope (SEM) (FEI Company, Hillsboro, Oregon, USA) [23].

2.6. Co-culture of cells

Cell co-culture was performed according to the protocol described by Qiu et al. [24]. The PCAECs and PCASMCs were grown separately to 70-80% confluence and isolated by 0.25% trypsin- EDTA solution. Cell suspensions were centrifuged for 5 min at 1000 rpm, then re-suspended in 1 mL of fresh culture medium without FBS. A green cell tracker (CMFDA) for labeling PCAECs and orange cell tracker (CMTMR) (Invitrogen, Waltham, MA, USA) for labeling PCASMCs were added to 1 mL PCAECs and 1 mL PCASMCs, respectively, with ratio of 1 uL tracker to 1 mL media and incubated at 37°C for 1 h with 5% CO_2 with humidification. After incubation, cells were centrifuged and washed twice with PBS. After the second wash, cells were re-suspended in DMEM (Gibco, Thermo Fisher Scientific, MA, USA) containing 4.5 g/L glucose, 4.5 g/L L-glutamine, 10% FBS, 100 U/mL penicillin, and 100 μg/mL streptomycin. Labeled cells were counted with a hemacytometer and combined to create a suspension of 50,000 total cells/mL consisting of

Author Manuscript Author Manuscript Author Manuscript Author Manuscript

a 50:50 mix of PCAECs and PCASMCs. Cells were seeded onto coupons placed inside 24-well plates. Culture media volume inside each well was 1 mL. Competitive cell proliferation and adhesion were examined with a Zeiss Axiovert 200M inverted fluorescence microscope (Carl Zeiss, Thornwood, NY, USA) after 1 day and 3 days. Cell numbers were counted by ImageJ software. At least 5 images with 10X magnification were taken on each sample and the results were averaged.

2.7. Cell migration

Cell migration tests were performed by using L-shaped CoCr L605 coupons as substrates (Figure 1). Horizontal and vertical parts of the L-shaped samples have the same dimensions (10 mm × 10 mm × 0.4 mm). The horizontal parts of all samples were uncoated. During plasma coating process, the horizontal parts were masked using other uncoated L605 coupons. The vertical parts were coated with either TMS plasma nanocoatings or NH_3/O_2 modified TMS plasma nanocoatings, which were identified as TMS and TMS + NH_3/O_2 plasma nanocoated L-shaped samples, respectively. Uncoated L605 L-shaped samples were used as control. All samples were placed in 24-well cell culture plates with uncoated L605 sides positioning on the bottom of the wells. Cells were seeded at a density of 16,000 cells/well and cultured for 24 hours to ensure formation of a confluent cell layer. After 24 hours, culture media were replaced with fresh media. After 7 days, samples were washed with PBS and fixed with sodium cacodylate (2% glutaraldehyde and 2% paraformaldehyde) at room temperature for 30 min. Cell migration over the treated vertical portion was inspected by an FEI Quanta 600 FEG Environmental SEM (FEI Company, Hillsboro, Oregon, USA).

2.8. Effect of ODQ on PCAMSC proliferation

1H-[1,2,4]oxadiazolo[4,3-a]quinoxalin-1-one (ODQ) irreversibly binds guanylate cyclase, which SMCs produce. Porcine coronary artery endothelial cells (PCAECs) were suspended and cultured in smooth muscle cell (SMC) culture medium, which was treated with ODQ or non-treated. Binding of ODQ occurs at a heme group that binds NO. When NO binds, cyclic guanine monophosphate (cGMP) is produced, which promotes the contractile phenotype of SMCs characterized by low rates of proliferation and migration. Stock ODQ (20 mM in DMSO) was diluted to 20 nM in smooth muscle cell culture medium. Control cells were treated with vehicle control. After 1- and 3-day incubation, PCASMC proliferation was determined quantitatively by MTT assay.

2.9. Platelet adhesion

An *in vitro* model was used to study platelet adhesion onto uncoated CoCr L605 coupons and TMS + NH_3/O_2 nanocoated coupons. Platelet attachment on coupon surfaces was observed by SEM. Under sterile conditions, porcine whole blood (containing Na heparin) from Innovative Research (Novi, MI, USA) was centrifuged (200 g, 15 min, 25 °C) to obtain platelet rich plasma (PRP). The specimens were then incubated in 24-well plates in 1 mL PRP at 37 °C for 2 hours. After incubation, samples were rinsed with PBS to remove non-adherent cells. For SEM analyses, specimens were fixed with sodium cacodylate at room temperature for 30 min and dried in an ethanol gradient, starting from 50% ethanol to 100%. Samples were kept in each ethanol dilution for 10 min followed by drying at room temperature.

Author Manuscript Author Manuscript Author Manuscript Author Manuscript

2.10. Clotting assay

Porcine whole blood from Innovative Research (Novi, MI, USA) contained Na heparin (diluted to 1 U/mL in whole blood). Under sterile conditions, the blood (3 mL) and DMEM/F12 (12 mL) were warmed separately to 37°C, then 1 part of blood was added to 3 parts of the whole DMEM/F12 medium. Samples (uncoated L605 coupons and TMS + NH_3/O_2 nanocoated coupons) were placed in a 24-well plate and sterilized under UV light for 15 min each side. One mL of the blood and DMEM/F12 mixture was added into each well containing a coupon sample. The 24-well plate was placed on a platform shaker (120 cycles/min) inside a 37°C incubator for 1 hour. After incubation, samples were rinsed well with PBS twice, then transferred to a new 24-well plate. Samples were fixed with buffered formalin at room temperature for 30 min and stained with crystal violet (CV) at room temperature for 10 min. A CV solution was made of 0.05 g CV powder (Fisher Scientific, Waltham, MA), 2 mL ethanol, and DI water to yield a final solution of 50 mL total. The CV stains the clot. The CV can detect all clotted material including fibrin and platelets. The stained specimens were rinsed thoroughly with DI water and PBS. An aliquot (1 mL) of glacial acid mixture (acid and DI water with 1:10 ratio) was added to each well containing samples and the cell plate was put onto the shaker for 10 min. The absorbance was measured at 595 nm.

2.11. *Ex vivo* perfusion chamber

An *ex vivo* perfusion chamber was used to study the effects of nanocoatings on platelet adhesion to coronary stents under physiologic sheer stress. Male domestic swine (15-30 kg) fed standard chow (Purina Lab Mini-pig Breeder Diet 5082) were used for whole blood collection. The protocol for blood collection was approved by the University of Missouri Animal Care and Use Committee. Swine were sedated by intramuscular injection of telazol (4.5 mg/kg) and xylazine (2 mg/kg), and, if necessary, inhalation of isoflurane (2-4%). The external jugular vein was cannulated with a 20G needle. Blood was withdrawn into a syringe and immediately transferred to a test tube containing lepirudin (a thrombin inhibitor, 25 μg/mL of whole blood). Porcine platelets from 40 mL of anticoagulated whole blood were labeled with Indium-111 by the tropolone method, as described [25-26]. Labeled platelets were washed and resuspended in 15 mL of lepirudin-anticoagulated whole blood obtained from the same animal.

Ex vivo perfusion circuit.—Clear, flexible peristaltic pump tubing (Masterflex L/S 14 #96419-14, I.D. 1.6 mm, Cole-Parmer Co.), length 80 cm, was flushed with acetone, allowed to dry, then flushed twice with Sigmacote (Sigma-Aldrich), allowing tubing to air dry between flushes. 316L stainless steel stents were positioned over a deflated balloon-tipped catheter (2.0 mm x 20 mm Maverick2 PTCA Dilatation Catheter, Boston Scientific, Marlborough, MA, USA) and deployed within the tubing by inflating the balloon to 5 atm for 30 seconds. For each experiment, different types of stents (uncoated [bare metal], coated only with TMS, or coated with TMS + NH_3/O_2, as described in Section 1.1) were placed in sequence in the tubing, allowing 3 cm between edges of adjacent stents, thus allowing comparison of platelet adhesion to stent struts under conditions of identical blood flow, platelet count, and indium labeling. Tubing containing stents was filled with 3 mL lepirudin-anticoagulated whole pig blood containing Indium-labeled platelets, taking care to avoid

Author Manuscript Author Manuscript Author Manuscript Author Manuscript

formation of any air bubbles within the tubing. A Sigmacote-treated hollow glass adapter was used to connect the ends of the tubing to create a closed circuit. Tubing was connected to a peristaltic pump (Masterflex console drive 7521-50 with L/S Easy-Load II pump head 77200-60, Cole-Parmer) and blood flow rate was adjusted to 6.9 mL/min, generating a shear rate of 67 s^{-1}, which is reflective of the sheer stress encountered in human coronary arteries *in vivo*. Flow was maintained for 30 minutes, during which the tubing was immersed in a heated water bath to maintain a temperature of 37°C. After stopping flow, the circuit was opened, blood was poured out and the tubing was gently flushed with 20 mL of PBS.

The segments of tubing containing each stent were individually excised (length of each segment was 12 mm), as were 3 segments (each 12 mm in length) of tubing that did not contain a stent, with one of the non-stented segments "upstream" of the stents, one "downstream," and one located between two of the stents (Figure 2). Radioactive counts per minute (CPM) of each segment of tubing were measured in a gamma counter (Wallac Wizard 3" 1480, PerkinElmer) with photon energy windows at 173 and 247 keV. To allow standardization of results between different experiments, the radioactive CPM of 10 μL of whole blood containing Indium-labeled platelets (i.e., from the same sample of labeled whole blood used to fill perfusion chamber tubing) was measured and the ratio of radioactive CPM in each tubing segment to the radioactive CPM of the 10 μL sample of labeled blood was calculated.

Total plasma protein adhesion.—To study potential mechanisms underlying the reduced platelet reactivity of the nanocoated stent, bare metal stents and nanocoated stents were inserted in the perfusion circuit, as described above, except that lepirudin-anticoagulated porcine platelet-poor plasma (PPP), rather than whole blood, was perfused over the stents for 30 min. Thereafter, stents were removed from the circuit tubing, rinsed extensively, and boiled in identical volumes of Laemmli buffer containing 2% sodium dodecyl sulfate (SDS) to elute bound plasma proteins, which were analyzed by sodium dodecyl-sulfate polyacrylamide gel electrophoresis (SDS-PAGE) and quantified by densitometric analysis of silver-stained gels using ImageJ software.

2.12. Statistical analysis

The data were all expressed as mean ± standard deviation (SD). Each experiment was repeated independently three times (n = 3), if not indicated otherwise. Data were analyzed using one-way ANOVA. A *p*-value of 0.05 or less was considered statistically significant.

3. Results and Discussion

3.1. Surface characterization

The measured thickness of TMS plasma nanocoatings was 20.5 ± 4.0 nm without plasma post-treatment, and 21.5 ± 3.8 nm after NH_3/O_2 plasma post-treatment. In these thickness ranges, the nanocoatings are highly conformal and do not affect the substrate topography [27-28]. As reported in our previous study [23], high magnification SEM images of the plasma nanocoated CoCr stents had the same surface morphology as that of the uncoated bare CoCr stents.

Author Manuscript Author Manuscript Author Manuscript Author Manuscript

The plasma nanocoatings were stable on immersion in a simulated body fluid of PBS for at least twelve weeks, as reported in our previous study [27]. The same plasma nanocoatings (TMS + NH_3/O_2) were deposited onto 316L stainless steel coupons and immersed in a simulated body fluid of PBS at 37 °C. After immersion for up to 12 weeks, the coatings were very stable in terms of water surface wettability and chemical composition/structures characterized by water contact angle measurements, XPS and Fourier-transform infrared spectroscopy (FTIR) analysis [27]. In contrast, stent endothelialization is expected to finish within three to four months post-implantation, limiting any degradation of the stent and nanocoating [29-31]. To assess long-term shelf storage stability of plasma nanocoatings, XPS surveys of CoCr alloy L605 coupon surfaces were performed 1 day, 1 year, and 2 years after the TMS + NH_3/O_2 nanocoating process. As shown in Figure 3A, all spectra showed similar peaks of O 1s (529 eV), N 1s (398 eV), C 1s (283 eV), Si 2p (152 eV), and Si 2s (99 eV). In contrast, as reported in our previous study [27], the XPS survey spectra of a clean CoCr alloy L605 surface showed mainly peaks of the CoCr alloy elements including Co 2p, Cr 2p, Ni 2p, W 4d, O 1s from surface metal oxides, but no N 1s and Si 2p peaks.

Table 1 summarizes the changes of chemical composition in NH_3/O_2 plasma post-treated TMS plasma nanocoatings aged for 1 day and 2 years. After 2-year aging, ratios of O 1s, N 1s, and C 1s to Si 2p were almost the same as those after 1-day aging, providing strong evidence for the surface chemical stability of NH_3/O_2 plasma post-treated TMS plasma nanocoatings. After 2-year aging, the increase of O 1s/Si 2p ratio from 1.292 to 1.413 can be attributed to the oxygen incorporation due to continuous oxidation of the plasma coatings in ambient air. The smaller increase of C 1s/Si 2p ratio from 0.756 to 0.832 can be attributed to carbon contamination when stored in ambient air to the surfaces.

Figure 3B shows the XPS core spectra of TMS + NH_3/O_2 plasma nanocoatings aged for 1 day and 2 years. It reveals the existence of characteristic peaks of N-C bonding at 395.65 eV and N-Si bonding at 397.43 eV [32-33]. The electronegativity of N is higher than that of C and Si, resulting in more electrons being pulled to cover N atom in N-C and N-Si bonds. Since electronegativity of Si was lower than that of C, more electrons were covered around N atom in N-Si bond than that in N-C bond. Therefore, the binding energy for N 1s was higher in N-Si bond, compared to N-C bond. These high-resolution scans confirm that nitrogen-containing groups are covalently bonded to the TMS-based nanocoating. In comparison with 1-day old plasma coatings, an increase in relative peak intensity ratio of N-Si/N-C was observed.

After stents are implanted in arteries, plasma proteins adhere to the strut surfaces. This process supports platelet adhesion, which is mediated by integrin and other receptors that bind plasma proteins, such as fibrinogen. The differences in surface energies between uncoated and TMS + NH_3/O_2 nanocoated stents would be expected to influence plasma protein adhesion to stent struts [34-35]. To examine this issue, uncoated 316L stainless steel stents and TMS + NH_3/O_2 nanocoated stents were placed within an *ex vivo* perfusion circuit containing porcine platelet-poor plasma (PPP) (Figure 2). Total blood plasma protein attachment was significantly lower on the TMS + NH_3/O_2 nanocoated stent compared to uncoated stent (Figure 4).

Author Manuscript Author Manuscript Author Manuscript Author Manuscript

As shown in Figure 5, for both PCAECs and PCASMCs, TMS nanocoating significantly inhibited cell viability compared to uncoated surfaces at all time points studied. TMS + NH_3/O_2 nanocoating yielded significantly greater cell viability for PCAECs at the 3-day and 7-day time points compared to TMS alone (Figure 5A), indicating that the post plasma treatment with NH_3/O_2 significantly accelerated endothelial cell recovery, producing a level of cell viability at day 7 that did not differ significantly from that of uncoated L605 surfaces. In contrast, for PCASMCs, TMS + NH_3/O_2 nanocoating did not significantly promote cell viability compared to TMS alone at any of the time points studied (Figure 5B), indicating that the post plasma treatment with NH_3/O_2 did not significantly enhance PCASMC viability. Therefore, compared to uncoated surface, TMS + NH_3/O_2 nanocoating significantly inhibited SMC viability at Day 7, while producing no inhibitory effect on endothelial cell viability. These results are significant, as they support the hypothesis that TMS + NH_3/O_2 nanocoating can be used to produce stents that inhibit SMC proliferation, like DES, while not disrupting endothelial cell recovery, a major limitation of DES.

The growth rates of PCAECs and PCASMCs were also examined by SEM, as shown in Figure 6. In agreement with the cell viability results in Figure 5, uncoated L605 surfaces were favorable for both PCAECs and PCASMCs, while TMS + NH_3/O_2 nanocoatings promoted PCAEC proliferation and at the same time inhibited PCASMC growth. SEM images show that PCAECs spread and grew robustly on uncoated L605 surface. Compared to PCAECs grown on uncoated L605 surfaces, PCAECs grown on TMS + NH_3/O_2 nanocoatings showed less density at day 1but became comparable at day 3 and very dense at day 7. From day 1 to day 7 of cell culture, very few PCASMCs were observed on TMS + NH_3/O_2 nanocoating surfaces, which exhibited a remarkable inhibitory effect on SMC adhesion compared to that on uncoated L605 surfaces. TMS plasma nanocoating without NH_3/O_2 plasma post-treatment yielded the lowest amount of PCAEC growth, which would not be beneficial for clinical stent applications. These results were consistent to the cell viability (MTT assay data), which showed that NH_3/O_2 modified TMS plasma nanocoating promotes PCAEC growth while inhibiting PCASMC attachment and proliferation.

3.2. Co-cell culture and cell migration

After stent implantation, the interaction between ECs and SMCs in coronary arteries plays a significant role in vascular wall remodeling and in-stent restenosis. Figure 7 displays fluorescent images and observed levels of adherent PCAECs and PCASMCs on uncoated L605 and plasma nanocoated coupons after 1-day and 3-day cell co-culture. Over the co-culture period, PCAEC proliferation and attachment on TMS + NH_3/O_2 nanocoatings were greatly enhanced compared to PCASMCs. Particularly, the cell ratio of PCAECs over PCASMCs on TMS + NH_3/O_2 nanocoatings was nearly 1.5-fold higher than those of uncoated cobalt chromium (CoCr) alloy L605 surfaces at both day 1 ($p < 0.005$) and day 3 ($p < 0.05$). This ratio enhancement demonstrates the selectivity of TMS + NH_3/O_2 nanocoatings for PCAEC growth.

After percutaneous coronary intervention (PCI), migration of endothelial cells is considered advantageous in terms of restoring an intact vascular endothelium, while migration of SMCs is considered disadvantageous, as it supports neointima formation and restenosis. The

Author Manuscript Author Manuscript Author Manuscript Author Manuscript

migration results of PCASMCs and PCAECs are shown in Figure 8. Migration distances of PCAECs on uncoated L605 and TMS + NH_3/O_2 nanocoated coupons were almost the same at 1.35 ± 0.29 mm and 1.38 ± 0.17 mm after 7 days, respectively. In contrast, significant difference in migration distances of PCASMCs was observed on TMS + NH_3/O_2 nanocoated and uncoated L605 samples. In particular, migration distance of PCASMCs on TMS + NH_3/O_2 nanocoatings decreased nearly 8.5-fold as compared to that on uncoated L605 surface ($p < 0.005$). The migration distance of PCAECs on TMS plasma nanocoating was much shorter than those on uncoated L605 and TMS + NH_3/O_2 nanocoatings ($p < 0.005$), indicating that TMS plasma coating without plasma post-treatment for surface modification yielded a surface that does not promote EC migration.

3.3. Effect of ODQ on PCASMC proliferation

The impact of NO on the cardiovascular system is related to its activation of soluble guanylate cyclase (sGC) [21,36], as well as effects on processes that are independent of sGC, including scavenging of superoxide anion and integrin activation [37]. Activation of sGC by NO generates cyclic guanosine monophosphate (cGMP), which leads to SMC relaxation, reduced SMC proliferation, enhancement of endothelial cell migration, and prevention of platelet adhesion and activation. Since it is a high affinity and potent inhibitor of sGC, ODQ inhibits NO-dependent generation of cGMP by sGC. As shown in Figure 9, addition of ODQ into culture media did not significantly affect PCASMC proliferation on uncoated L605 surfaces at both day 1 and day 3. However, at day 3 incubation in culture medium containing ODQ, the number of viable PCASMCs grown on TMS + NH_3/O_2 nanocoating surfaces was 95% higher ($p < 0.05$) compared to those incubated without ODQ. The results suggested that, on TMS + NH_3/O_2 plasma nanocoating surfaces, there might exist N- and O-containing chemical groups capable of mimicking the effects of NO on sGC and inhibiting PCASMC growth. In our previous study [27], we observed nitrite ester (-C-O-N=O) chemical groups on the FTIR spectra of the same TMS + NH_3/O_2 plasma coating deposited onto 316L stainless steel coupons.

Cell migration and proliferation of PCAECs and PCASMCs on TMS plasma nanocoated samples without NH_3/O_2 plasma post-treatment were limited, most likely due to their hydrophobicity, which is not favorable for cell growth and migration. As reported in our recent study [23], TMS plasma coating had a hydrophobic surface with a water contact angle of 99°. In contrast, the fresh TMS + NH_3/O_2 nanocoating surface was very hydrophilic with a water contact angel of a quick hydrophobic recovery from < 5° on a fresh coating surface increased to near 20° in the first 24-hour period, then gradually increased to nearly 45° after 24 weeks, and finally stabilized around 48.5° for 2 years. TMS + NH_3/O_2 nanocoatings, which had moderate water contact angles, are considered favorable for cell growth [23]. Reduced binding of plasma proteins, such as fibrinogen, vitronectin, and fibronectin, to which endothelial cells and SMCs bind, can also account for the reduced binding of cells to nano-coated surfaces. On the other hand, TMS + NH_3/O_2 plasma nanocoatings showed selectivity of enhancing PCAEC proliferation and migration while at the same time inhibiting PCASMC proliferation and migration. Such selectivity is key for successful coronary stent applications to accomplish the regeneration of a healthy endothelium while inhibiting restenosis.

Author Manuscript Author Manuscript Author Manuscript Author Manuscript

3.4. Platelet adhesion and blood clotting

Platelet adhesion and activation are major indicators of the hemocompatibility of devices implanted in the vasculature, such as coronary stents. Platelet adhesion tests were performed on uncoated L605 and plasma nanocoated coupons and stents to study the effects of plasma nanocoatings on platelet attachment and activation. Figure 10A presents SEM images of adhered platelets on uncoated L605 and TMS + NH_3/O_2 samples after being subjected to immersion in PRP at 37°C for 2 h. On TMS + NH_3/O_2 plasma nanocoated coupon surfaces, platelets remained isolated and showed low distribution, whereas greater platelet adhesion and clustering was observed on uncoated L605 surfaces. At higher magnification, platelets are 5 μm in size and are dendritic or discoid in shape. Adhered platelets on uncoated L605 surfaces are more activated with surrounding short pseudopodia, suggesting the beginning state of platelet activation. Compared to platelets on uncoated L605, adhered platelets on TMS + NH_3/O_2 nanocoated surfaces were more in discoid shape, consistent with a less activated state. In Figure 10B, adhered platelet density on TMS + NH_3/O_2 plasma nanocoated coupons (about 150 ± 17 platelets/mm^2) was 70 ± 16% lower ($p < 0.005$) than that on uncoated L605 surfaces (about 600 ± 131 platelets/mm^2). Similarly, SEM images in Figure 10C indicate that, on uncoated L605 stents, many dendritic platelets gather mostly at the edges of stent struts, dispersing throughout strut area. In contrast, almost no platelets were detected on NH_3/O_2 treated TMS plasma coated stent surfaces. The amount of whole blood clotting on TMS + NH_3/O_2 nanocoated surfaces was 54 ± 12% ($p < 0.05$) that of uncoated L605 surface in Figure 10D, suggesting that TMS + NH_3/O_2 plasma coatings inhibit whole blood clotting on metal surfaces. In clinical situations, stent implantation increases platelet activation [38-39]. Thus, the ability of TMS + NH_3/O_2 plasma nanocoatings to hinder platelet activation may play a decisive role in thrombosis prevention.

Shearing stresses strongly influence platelet activation [35,39-40]. To study the anti-adhesive properties of the nanocoating under conditions more reflective of those encountered *in vivo*, coronary stents were deployed in a closed-circuit *ex vivo* perfusion circuit to quantify adhesion of indium-labeled platelets to stents under physiologic shear stress of blood flow. Platelet adhesion to bare metal 316L SS stents, TMS, and TMS + NH_3/O_2 nanocoated 361L SS stents was assessed by measuring radioactive CPM of indium-111 platelets adhering to stents during perfusion of anticoagulated whole blood within the perfusion circuit. The TMS + NH_3/O_2 nanocoated stents showed significantly lower platelet adhesion under simulated physiological blood flow conditions (Figure 11A). SEM analysis of the stents from the perfusion circuit confirmed the low level of platelet adhesion to TMS + NH_3/O_2 plasma nanocoatings (Figure 11B). Thus, under shear stress conditions, TMS + NH_3/O_2 nanocoating significantly inhibited platelet adhesion compared to the uncoated 316L stents and TMS nanocoated 316L SS stents. The data are consistent with the hypothesis that TMS + NH_3/O_2 nanocoating inhibits platelet activation by the following mechanisms, i.e., 1) inhibition of binding of plasma proteins, such as fibrinogen, to metal surfaces, and 2) generation of N- and O-containing chemical groups on the nanocoated surface capable of mimicking the inhibitory effects of NO on platelet adhesion and activation. Chen et al. showed that a similar NH_3/O_2 plasma treatment onto 316L stainless steel suppressed the surface platelet attachment [41]. Furthermore, the same NH_3/O_2 plasma treatments, when

Author Manuscript Author Manuscript Author Manuscript Author Manuscript

applied to polytetrafluoroethylene (PTFE), promoted extensive endothelial cell proliferation [42].

In the plasma state, NH_3 and O_2 can react to form NO and other N- and O-containing chemical groups, which covalently bond to TMS plasma nanocoating. We hypothesize the NH_3/O_2 plasma post-treatment process employed in our study generated NO chemical groups covalently bonded to TMS plasma nanocoating (TMS-bonded NO), which may induce biologic signaling in vascular ECs, SMCs, and blood platelets without existing in a gaseous, diffusible state. While we demonstrated that the NH_3/O_2 plasma post-treatment process resulted in accumulation of nitrogen and oxygen on the TMS plasma nanocoating surface, a limitation of our study is that we could not confirm experimentally the presence of TMS-bonded NO. Nevertheless, we have shown that the NH_3/O_2 plasma post-treatment process confers on TMS plasma nanocoating with biologic properties that mimic those of NO. While TMS-bonded NO would not be expected to diffuse into the cytoplasm of cells to activate sGC, we showed that ODQ, an inhibitor of sGC, effectively inhibited the biologic effect of the TMS + NH_3/O_2 plasma nanocoating. Currently, we do not have an adequate explanation for this intriguing finding. Independent of potential effects on sGC, TMS-bonded NO could possibly mimic some of the recognized extracellular functions of NO, including scavenging superoxide anion to form peroxynitrite and inhibiting of integrin activation. Additional experiments, which are beyond the scope of this study, are needed to clarify 1) the extent to which NO accumulates on the TMS plasma coating surface during the NH_3/O_2 plasma post-treatment process, and 2) the biologic functionality of this immobilized pool of NO.

4. Conclusions

NH_3/O_2 plasma modified TMS plasma nanocoatings (TMS + NH_3/O_2 nanocoatings) were successfully fabricated onto CoCr alloy L605 surfaces and 316L surfaces. The *in vitro* results obtained in this study revealed that TMS + NH_3/O_2 nanocoatings with hydrophilic surfaces containing N and O elements exhibited good biocompatibility and hemocompatibility. The TMS + NH_3/O_2 nanocoating accelerated proliferation and migration of coronary artery ECs while inhibiting attachment, proliferation, and migration of coronary artery SMCs, and reducing platelet adhesion and activation. Therefore, TMS + NH_3/O_2 nanocoatings are very promising in coronary stent applications to prevent both restenosis and thrombosis.

Funding:

This research was funded by the National Institutes of Health (NIH) (Grant number: 5R44HL097485).

References

[1]. Ahmad F, Anderson R, 2021, The Leading Causes of Death in the US for 2020, JAMA 325(18), 1829–1830. [PubMed: 33787821]

[2]. Ralapanawa U, Sivakanesan R, 2021, Epidemiology and the Magnitude of Coronary Artery Disease and Acute Coronary Syndrome: A Narrative Review, Journal of Epidemiology and Global Health, 11(2) 169–177. [PubMed: 33605111]

Author Manuscript Author Manuscript Author Manuscript Author Manuscript

[3]. Hu T, Yang C, Lin S, Yu Q and Wang G, 2018, Biodegradable stents for coronary artery disease treatment: Recent advances and future perspectives, Materials Science and Engineering C 91, 163–178. [PubMed: 30033243]

[4]. Curcio A, Torella D and Indolfi C, 2011, Mechanisms of smooth muscle cell proliferation and endothelial regeneration after vascular injury and stenting, Circulation Journal, 75, 1287–96. [PubMed: 21532177]

[5]. Lyu N, Du Z, Qiu H, Gao P, Yao Q, Xiong K, Tu Q, Li X, Chen B, Wang M, Pan G, Huang N and Yang Z, 2020, Mimicking the Nitric Oxide-Releasing and Glycocalyx Functions of Endothelium on Vascular Stent Surfaces, Advanced Science 7 (21).

[6]. Sun D, Zheng Y, Yin T, Tang C, Yu Q and Wang G, 2014, Coronary drug-eluting stents: From design optimization to newer strategies, Journal of Biomedical Materials Research - Part A 102, 1625–40. [PubMed: 23703913]

[7]. Babapulle MN and Eisenberg MJ, 2002, Coated stents for the prevention of restenosis: Part I, Circulation 106, 2734–40. [PubMed: 12438301]

[8]. Holmes DR, Kereiakes DJ, Garg S, Serruys PW, Dehmer GJ, Ellis SG, Williams DO, Kimura T and Moliterno DJ, 2010, Stent Thrombosis, Journal of the American College of Cardiology 56, 1357–65. [PubMed: 20946992] [16]Seeger JM, Bigatan E, Klingman N, Amery D, Widenhouse C and Goldberg EP, 1995, Hydrophilic surface endoluminal stents modification of metallic, Journal of Vascular Surgery, 22 (3), 327–336. [PubMed: 7674476]

[9]. Urban P, Meredith IT, Abizaid A, Pocock SJ, Carrié D, Naber C, Lipiecki J, Richardt G, Iñiguez A, Brunel P, Valdes-Chavarri M, Garot P, Talwar S, Berland J, Abdellaoui M, Eberli F, Oldroyd K, Zambahari R, Gregson J, Greene S, Stoll H-P and Morice M-C, 2015, Polymer-free Drug-Coated Coronary Stents in Patients at High Bleeding Risk, New England Journal of Medicine 373, 2038–47. [PubMed: 26466021]

[10]. Simard T, Hibbert B, Ramirez FD, Froeschl M, Chen YX and O'Brien ER, 2014, The Evolution of Coronary Stents: A Brief Review, Canadian Journal of Cardiology 30, 35–45. [PubMed: 24286961]

[11]. Shim JW, Bae IH, Park DS, Lim KS, Lee SY, Jang EJ, Park JK, Kim JH and Jeong MH, 2017, Evaluation of ion implantation for anti-thrombogenic coronary stent in vitro and in vivo, Journal of Industrial and Engineering Chemistry 54, 290–297.

[12]. Cook S, Ladich E, Nakazawa G, Eshtehardi P, Neidhart M, Vogel R, Togni M, Wenaweser P, Billinger M, Seiler C, Gay S, Meier B, Pichler WJ, Jüni P, Virmani R and Windecker S, 2009, Correlation of Intravascular Ultrasound Findings With Histopathological Analysis of Thrombus Aspirates in Patients With Very Late Drug-Eluting Stent Thrombosis, Circulation, 120, 391–399. [PubMed: 19620501]

[13]. Reejhsinghan R, Lotfi A, 2015, Prevention of stent thrombosis: challenges and solutions, Vascular Health and Risk Management, 11, 93–106. [PubMed: 25657588]

[14]. Taniwaki M, Radu M, Zaugg S, Amabile N, Garcia-Garcia HM, Yamaji K, Jørgensen E, Kelbæk H, Pilgrim T, Caussin C, Zanchin T, Veugeois A, Abildgaard U, Jüni P, Cook S, Koskinas KC, Windecker S, Räber L, 2016, Mechanisms of Very Late Drug-Eluting Stent Thrombosis Assessed by Optical Coherence Tomography, Circulation, 133(7), 650–660. [PubMed: 26762519]

[15]. Jinnouchi H, Sato Y, Cheng Q, Janifer C, Kutyna M, Cornelissen A, Wijeratne R, Sakamoto A, Guo L, Kolodgie FD, Tunev S, Virmani R and Finn A, 2021, Thromboresistance and endothelial healing in polymer-coated versus polymer-free drug-eluting stents: Implications for short-term dual anti-platelet therapy, International Journal of Cardiology 327, 52–57. [PubMed: 33242506]

[16]. Bricout N, Chai F, Sobocinski J, Hertault A, Laure W, Ung A, Woisel P, Lyskawa J and Blanchemain N, 2020, Immobilisation of an anti-platelet adhesion and anti-thrombotic drug (EP224283) on polydopamine coated vascular stent promoting anti-thrombogenic properties, Materials Science and Engineering C 113, 110967. [PubMed: 32487386]

[17]. Zhang Y, Wang X, Ma Z, Bai B, Liu J, Yang L, Qin G and Zhang E, 2020, A potential strategy for in-stent restenosis: Inhibition of migration and proliferation of vascular smooth muscle cells by Cu ion, Materials Science and Engineering C 115, 111090. [PubMed: 32600694]

[18]. Capodanno D, Bhatt D, Gibson C, James S, 2022, Bleeding avoidance strategies in percutaneous coronary intervention, Nature Reviews Cardiology 19, 117–132. [PubMed: 34426673]

Author Manuscript Author Manuscript Author Manuscript Author Manuscript

[19]. Varenne O, Cook S, Sideris G, Kedev S, Cuisset T, 2018, Drug-eluting stents in elderly patients with coronary artery disease (SENIOR): a randomized single-blind trial, The Lancet, 391(10115), 41–50.

[20]. Barbato JE and Tzeng E, 2004, Nitric oxide and arterial disease, Journal of Vascular Surgery 40, 187–93. [PubMed: 15218485]

[21]. Rao J, Pan Bei H, Yang Y, Liu Y, Lin H and Zhao X, 2020, Nitric Oxide-Producing Cardiovascular Stent Coatings for Prevention of Thrombosis and Restenosis, Frontiers in Bioengineering and Biotechnology 8, 578–588. [PubMed: 32671029]

[22]. Bowles DK, Graier WF, Sturek M, 2001, Hydrogen peroxide activates Na^+-dependent Ca^{2+} influx in coronary endothelial cells, Biochemical and Biophysical Research Communications, 287, 1134–1139. [PubMed: 11587541]

[23]. Phan T, Jones JE, Chen M, Bowles DK, Fay WP, and Yu Q, 2022, "A biocompatibility study of Plasma nanocoatings onto Cobalt Chromium L605 alloys for Cardiovascular stent applications", Materials, 15(17), 5968. [PubMed: 36079346]

[24]. Qiu H, Qi P, Liu J, Yang Y, Tan X, Xiao Y, Maitz MF, Huang N and Yang Z, 2019, Biomimetic engineering endothelium-like coating on cardiovascular stent through heparin and nitric oxide-generating compound synergistic modification strategy, Biomaterials 207, 10–22. [PubMed: 30947118]

[25]. Dewanjee MK, Shyam AR, Didisheim P, 1981, Indium-i 11 Tropolone, A New High-AffinityPlateletLabel: Preparationand Evaluation of LabelingParameter, The journal of Nuclear Medicine: Basic Sciences – Radiochemistry and Radiopharmaceuticals 22, 981–987.

[26]. Kotze HF, Heyns AP, Lotter MG, Pieters H, Roodt JP, Sweetlove MA, Badenhorst PN, 1991, Comparison of Oxine and Tropolone Methods for Labeling Human Platelets with Indium- 11, The journal of Nuclear Medicine 32(1), 62–66. [PubMed: 1899112]

[27]. Jones JE, Yu Q, Chen M, 2017, A chemical stability study of trimethylsilane plasma nanocoatings for coronary stents, Journal of Biomaterials Science, Polymer Edition, 28(1).

[28]. Ma Y, Chen M, Jones JE, Ritts AC, Yu Q, Sun H, 2012, Inhibition of Staphylococcus epidermidis biofilm by trimethylsilane plasma coating, Antimicrob Agents Chemother, 56(11), 5923–37. [PubMed: 22964248]

[29]. Habib A and Finn AV, 2015, Endothelialization of Drug Eluting Stents and its Impact on Dual Anti-platelet Therapy Duration, Pharmacol Res., 93, 22–27. [PubMed: 25533811]

[30]. Nakazawa G, 2011, Stent thrombosis of drug eluting stent: Pathological perspective, Journal of Cardiology, 58, 84–91. [PubMed: 21839616]

[31]. Farb A, Burke A, Kolodgie FD, Virmani R, 2003, Pathological Mechanisms of Fatal Late Coronary Stent Thrombosis in Humans, Circulation, 108, 1701–1706 [PubMed: 14504181]

[32]. Yang DQ and Sacher E, 2003, A spectroscopic study of CNx formation by the keV N_2^+ irradiation of highly oriented pyrolytic graphite surfaces, Surface Science 531(2), 185–98.

[33]. Rosenberger L, Baird R, McCullen E, Auner G and Shreve G, 2008, XPS analysis of aluminum nitride films deposited by plasma source molecular beam epitaxy, Surface and Interface Analysis 40, 1254–61.

[34]. Milleret V, Ziogas A, Buzzi S, Heuberger R, Zucker A and Ehrbar M, 2015, Effect of oxide layer modification of CoCr stent alloys on blood activation and endothelial behavior, Journal of Biomedical Materials Research - Part B Applied Biomaterials 103, 629–40. [PubMed: 24964763]

[35]. Jaganathan SK, Supriyanto E, Murugesan S, Balaji A, and Asokan MK, 2014, Biomaterials in Cardiovascular Research: Applications and Clinical Implications, BioMed Research International, 2014 (1), 1–11.

[36]. Yang Z, Yang Y, Xiong K, Li X, Qi P, Tu Q Huang N, 2015, Nitric oxide producing coating mimicking endothelium function for multifunctional vascular stents. Biomaterials, 63, 80–92. [PubMed: 26093790]

[37]. Szabó C, Ischiropoulos H, and Radi R, 2007, Peroxynitrite: biochemistry, pathophysiology and development of therapeutics, Nature Reviews Drug Discovery, 6, 662–680. [PubMed: 17667957]

[38]. Marcondes S, Cardoso MHM, Morganti RP, Thomazzi SM, Lilla S, Murad F, de Nucci G and Antunes E, 2006, Cyclic GMP-independent mechanisms contribute to the inhibition of

Author Manuscript Author Manuscript Author Manuscript Author Manuscript

platelet adhesion by nitric oxide donor: A role for α-actinin nitration, PNAS 103(9), 3434–3439. [PubMed: 16492779]

[39]. Carvajal JA, Germain AM, Huidobro-Toro JP and Weiner CP, 2000, Molecular Mechanism of cGMP-Mediated Smooth Muscle Relaxation, Journal of Cellular Physiology, 184(3), 409–420. [PubMed: 10911373]

[40]. Tepe G, Wendel HP, Khorchidi S, Schmehl J, Wiskirchen J, Pusich B, Claussen CD and Duda SH, 2002, Thrombogenicity of Various Endovascular Stent Types: An In Vitro Evaluation, Journal of Vascular and Interventional Radiology, 13(10), 1029–1035. [PubMed: 12397125]

[41]. Chen M, Zamora PO, Peña L, Som P and Osaki S, 2003, NH_3/O_2 mixed gas plasmas alter the interaction of blood components with stainless steel, J. Biomed. Mater. Res, 67A, 994–1000.

[42]. Chen M, Zamora PO, Som P, Peña LA, & Osaki S, 2003, Cell attachment and biocompatibility of polytetrafluoroethylene (PTFE) treated with glow-discharge plasma of mixed ammonia and oxygen, Journal of Biomaterials Science, Polymer Edition, 14(9), 917–935. [PubMed: 14661870]

Author Manuscript Author Manuscript Author Manuscript Author Manuscript

Highlights

- The plasma nanocoatings with NH_3/O_2 plasma post-treatment (TMS + NH_3/O_2) promoted cell proliferation and migration of porcine coronary artery endothelial cells (PCAECs), and at the same time inhibited cell proliferation and migration of porcine coronary artery smooth muscle cells (PCASMCs).
- The nanocoatings of TMS + NH_3/O_2 showed much improved hemocompatibility with 70% lower platelet adhesion, 54% reduced clotting attachment, and less platelet activation as compared to uncoated L605 surfaces.
- The nanocoatings of TMS + NH_3/O_2 are very promising in preventing both restenosis and thrombosis for coronary stent applications.

Author Manuscript Author Manuscript Author Manuscript Author Manuscript

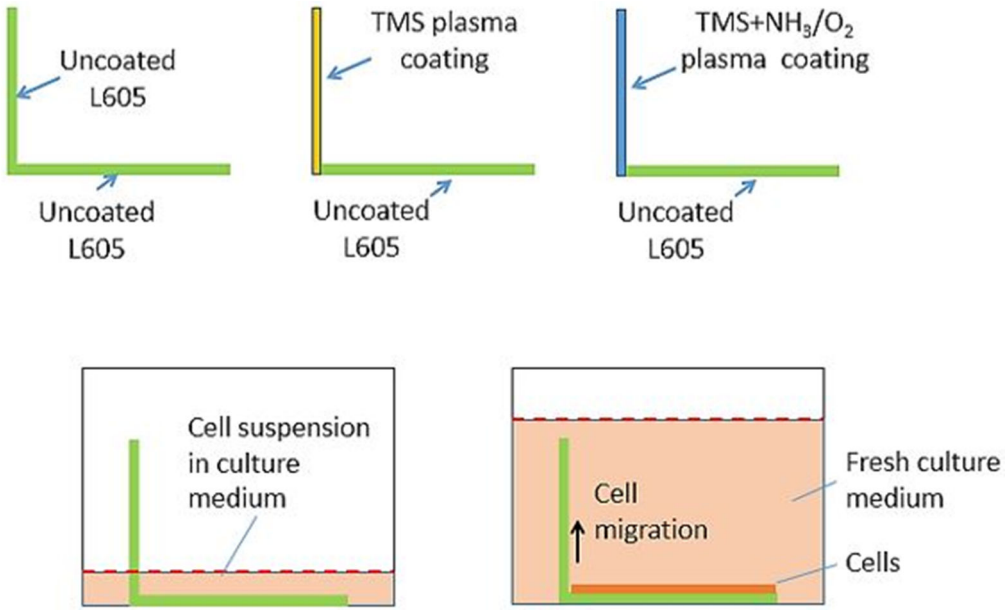

Figure 1:
Schematic diagram for cell migration test.

Author Manuscript Author Manuscript Author Manuscript Author Manuscript

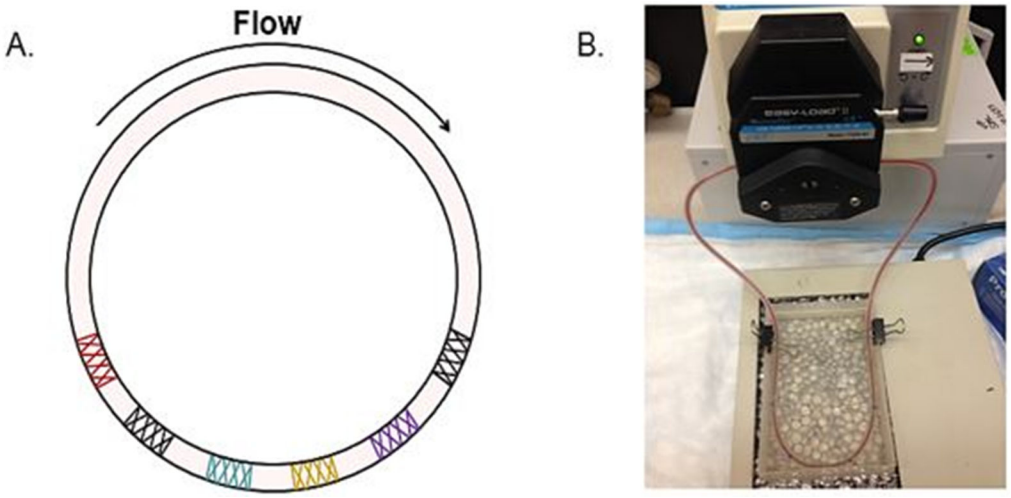

Figure 2:
A) Stents were placed tubing in a random order; B) Experimental system showing peristaltic pump and warming bath.

Author Manuscript Author Manuscript Author Manuscript Author Manuscript

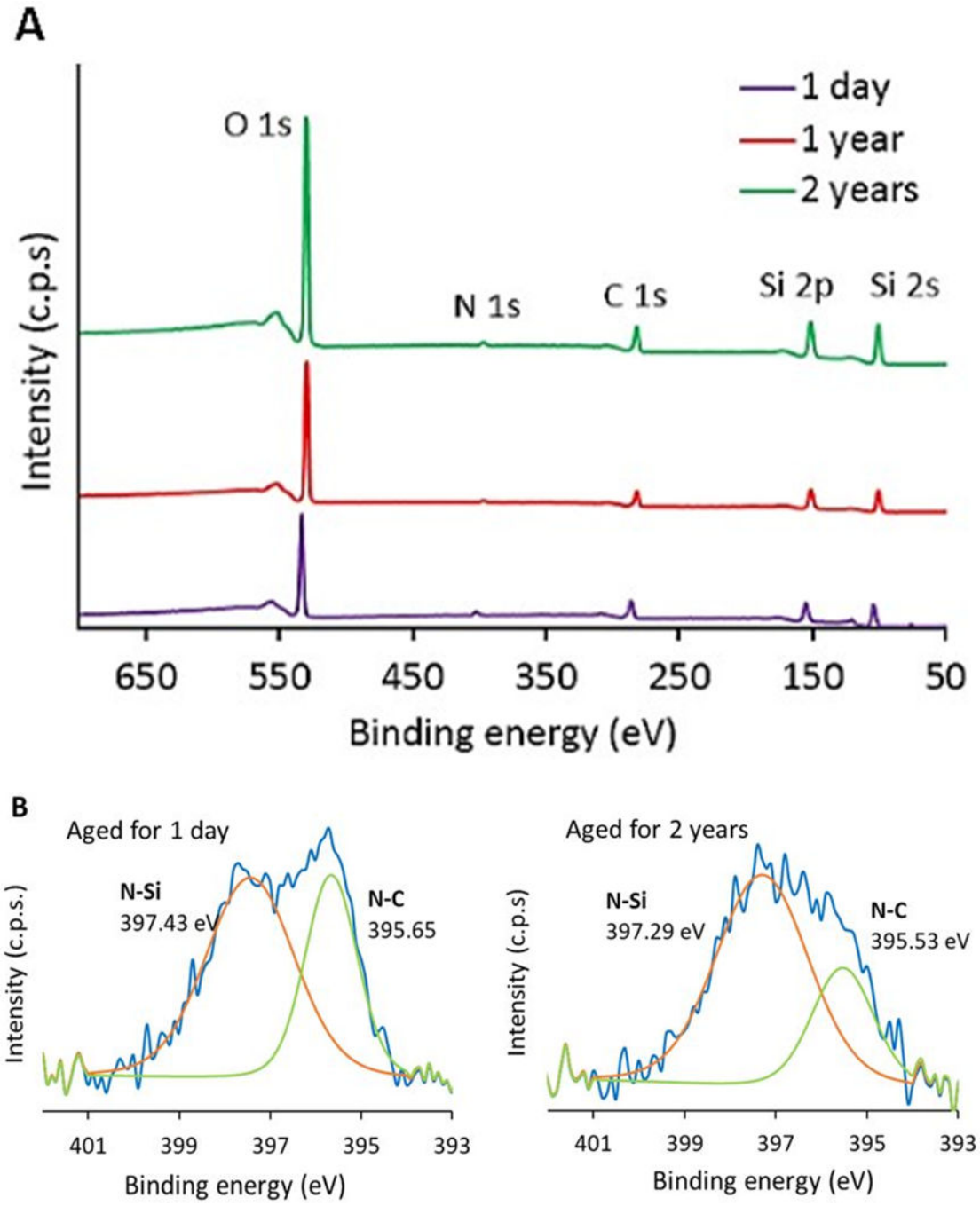

Figure 3:

A) XPS survey spectra of TMS + NH_3/O_2 plasma nanocoatings aged for 1 day, 1 year and 2 years; B) N1s core-level spectra of TMS + NH_3/O_2 plasma nanocoatings aged for 1 day and 2 years, n =3.

Author Manuscript Author Manuscript Author Manuscript Author Manuscript

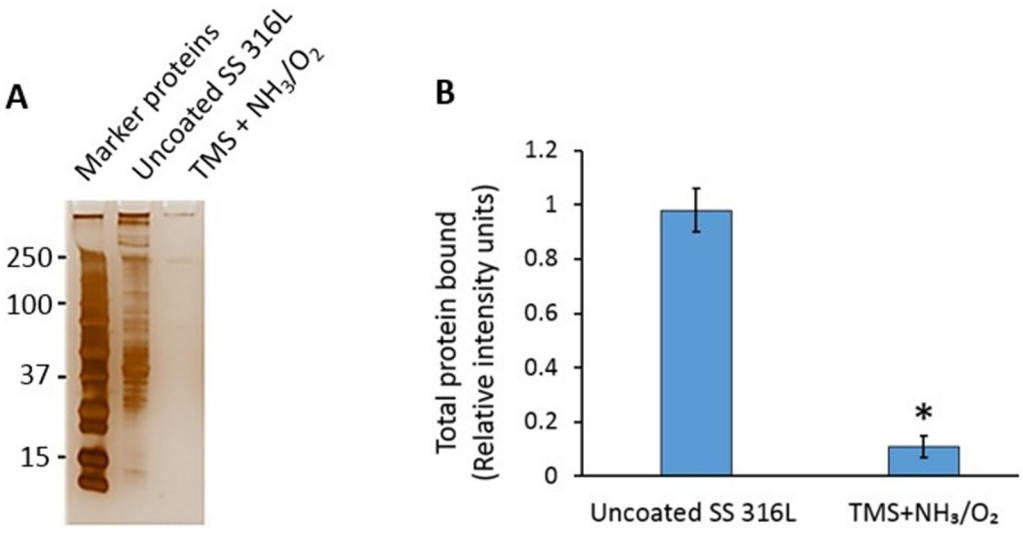

Figure 4:

Binding of plasma proteins to NH_3/O_2 modified TMS plasma nanocoated 316L SS stents is significantly less than to uncoated 316L SS stents. a) Platelet-poor plasma (PPP) was perfused over stents for 30 min (n =3); b) Total protein bound to gels was quantified by densitometric analysis of silver-stained gels. Results shown are mean of triplicate experiments (* $p < 0.05$).

Author Manuscript Author Manuscript Author Manuscript Author Manuscript

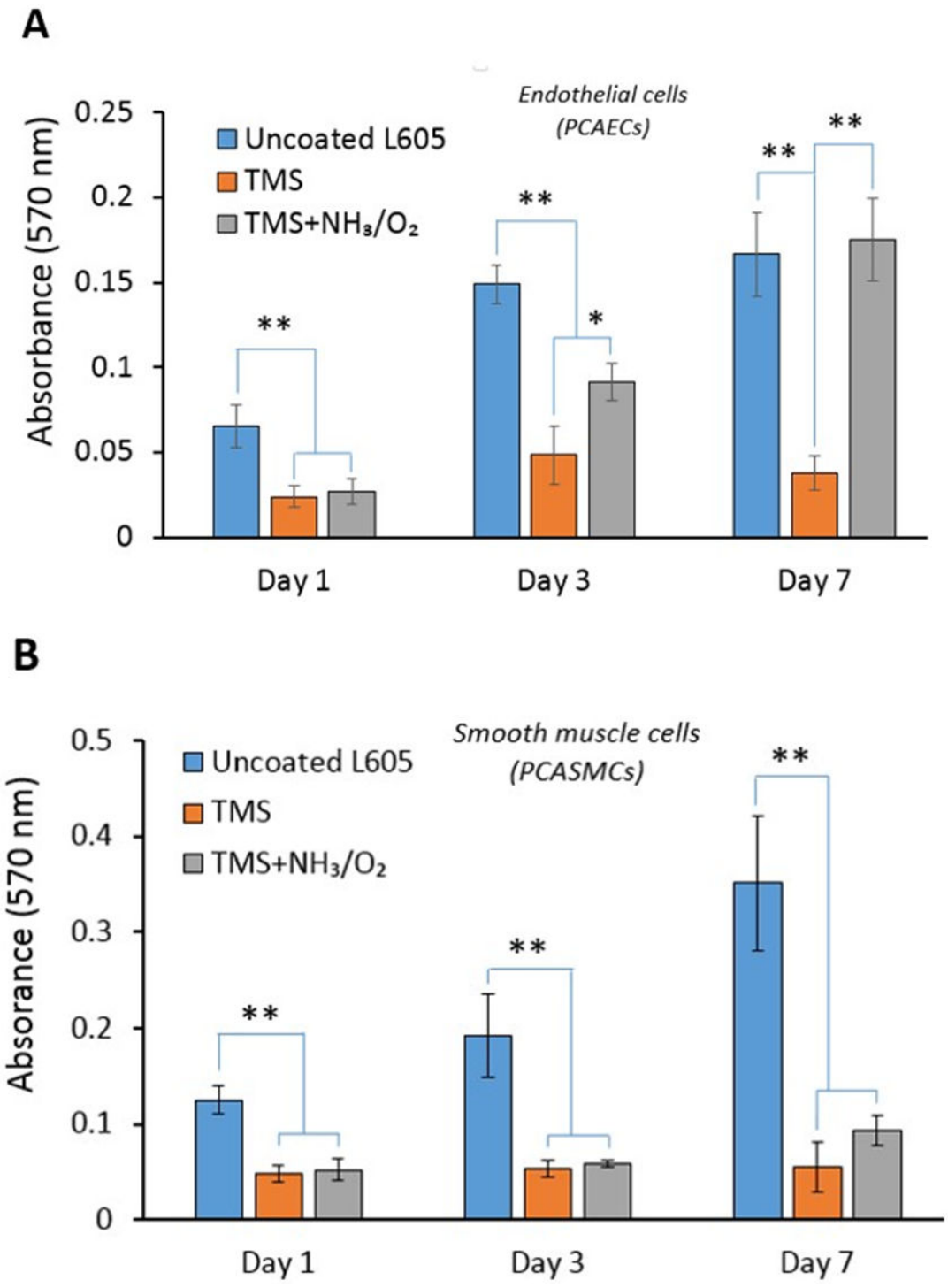

Figure 5:

Cell viability by MTT assay for A) PCAECs and B) PCASMCs after 1-, 3-, 7-day incubation on uncoated L605, TMS, and TMS + NH_3/O_2 plasma nanocoated coupons. Plotted values are means ±SD (n=6), *$p < 0.05$ and **$p < 0.005$.

Author Manuscript Author Manuscript Author Manuscript Author Manuscript

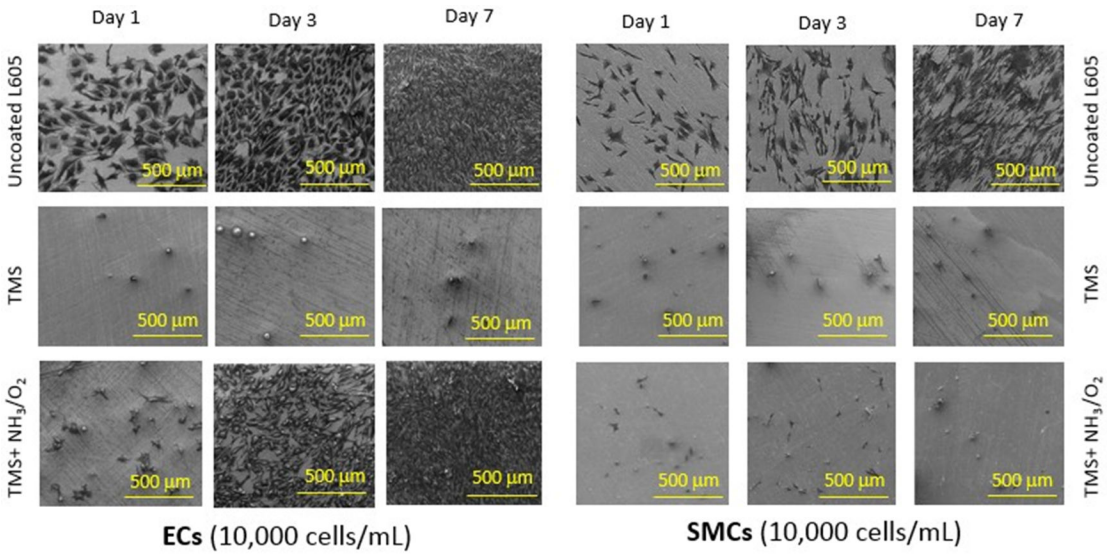

Figure 6:

SEM images for PCAEC and PCASMC attachment and proliferation onto uncoated L605, TMS, and TMS + NH_3/O_2 plasma nanocoatings after 1-, 3-, 7-day incubation (scale bar = 500 μm). Images shown are representative data obtained from 3 independent experiments.

Author Manuscript Author Manuscript Author Manuscript Author Manuscript

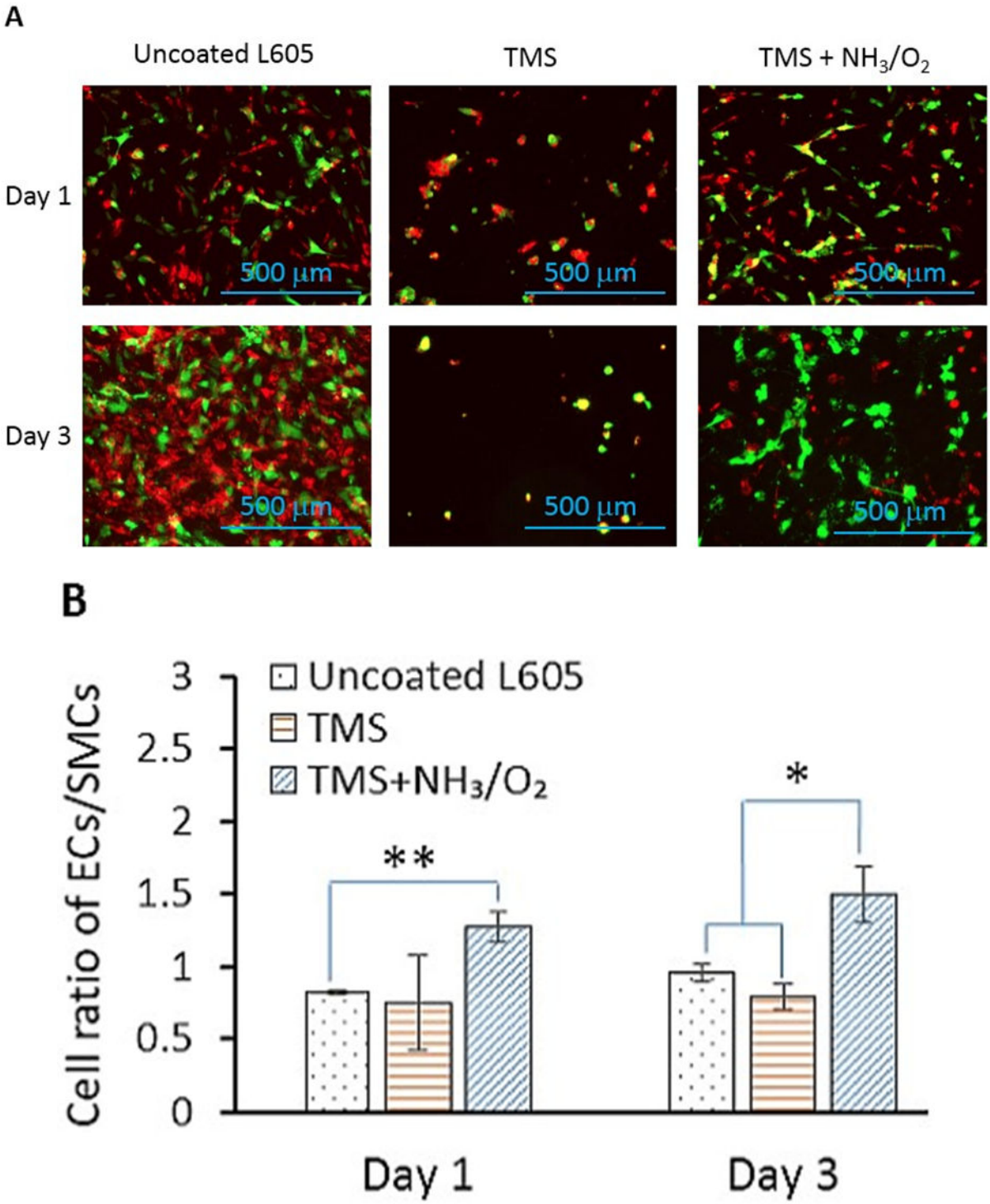

Figure 7:

A) Fluorescent micrographs showing PCAECs and PCASMCs proliferation and adhesion onto uncoated L605, TMS, and TMS + NH_3/O_2 plasma nanocoatings after 1 and 3 days. B) PCAEC/PCASMC cell ratio determined from the fluorescent micrographs by ImageJ. Data shown are mean ± SD (n = 6), *$p < 0.05$, **$p < 0.005$.

Author Manuscript Author Manuscript Author Manuscript Author Manuscript

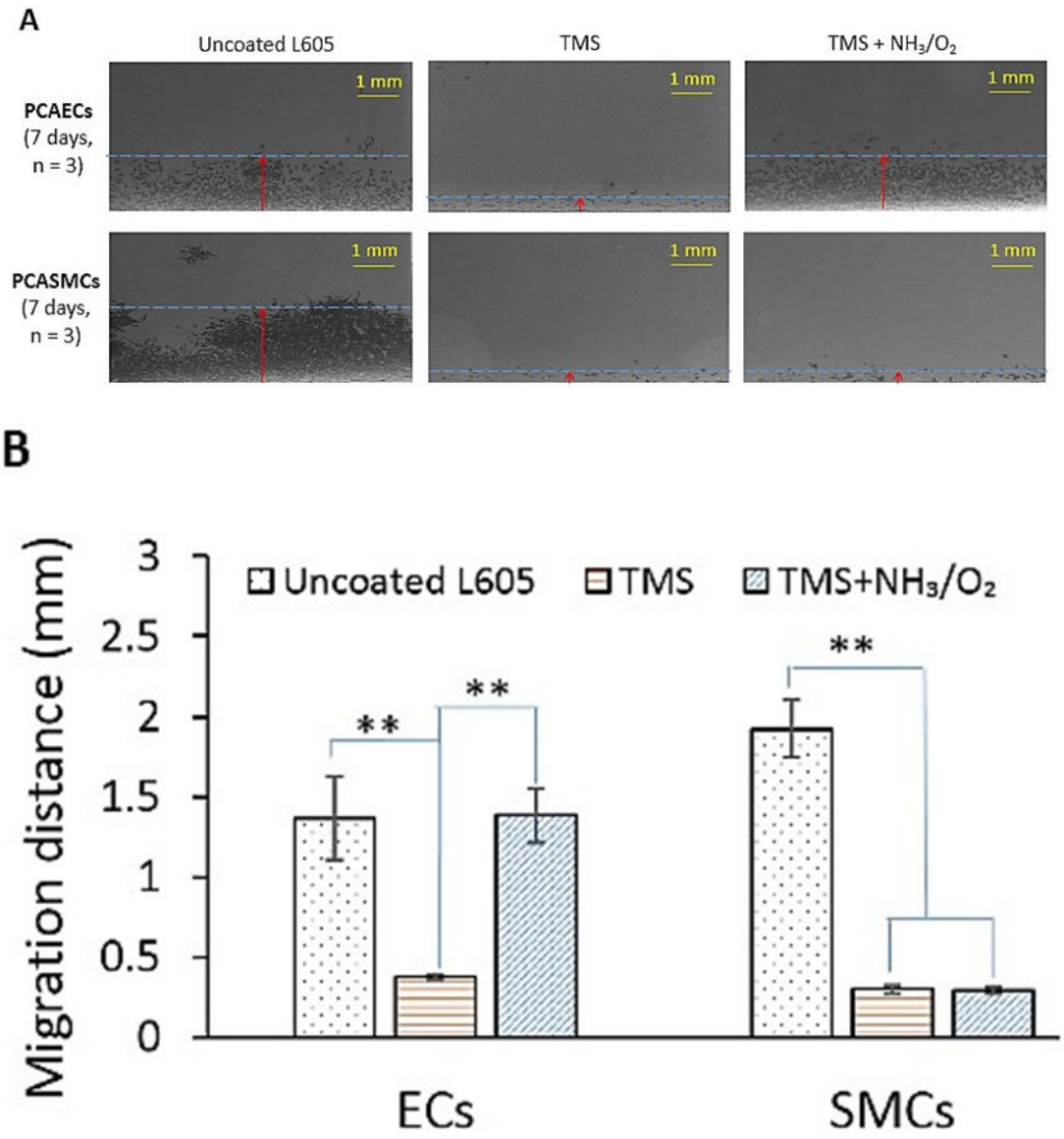

Figure 8:

A) Migration of PCAECs and PCASMCs on uncoated L605, TMS, and TMS + NH_3/O_2 plasma nanocoatings after 7 days. B) Migration distances determined by ImageJ. Data shown are mean ± SD (n = 6), $^{**}p < 0.005$.

Author Manuscript Author Manuscript Author Manuscript Author Manuscript

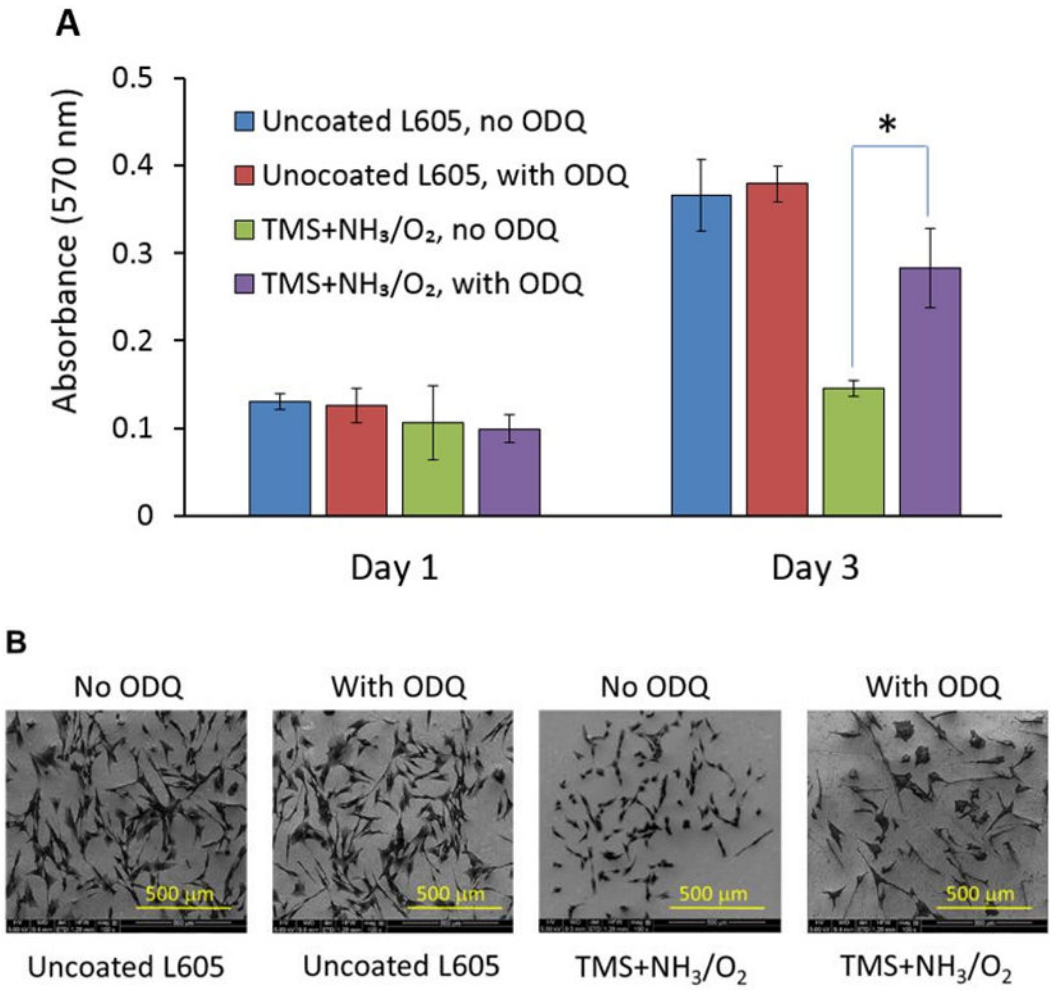

Figure 9:

A) PCASMC viability level with and without adding ODQ solution, evaluated by MTT assay, on uncoated L605 and TMS + NH_3/O_2 plasma nanocoatings, at day 1 and day 3. Plotted values are means ±SD (n=6), *$p < 0.05$; B) SEM images for PCASMC growth on uncoated L605 and plasma nanocoatings with and without adding ODQ solution.

Author Manuscript Author Manuscript Author Manuscript Author Manuscript

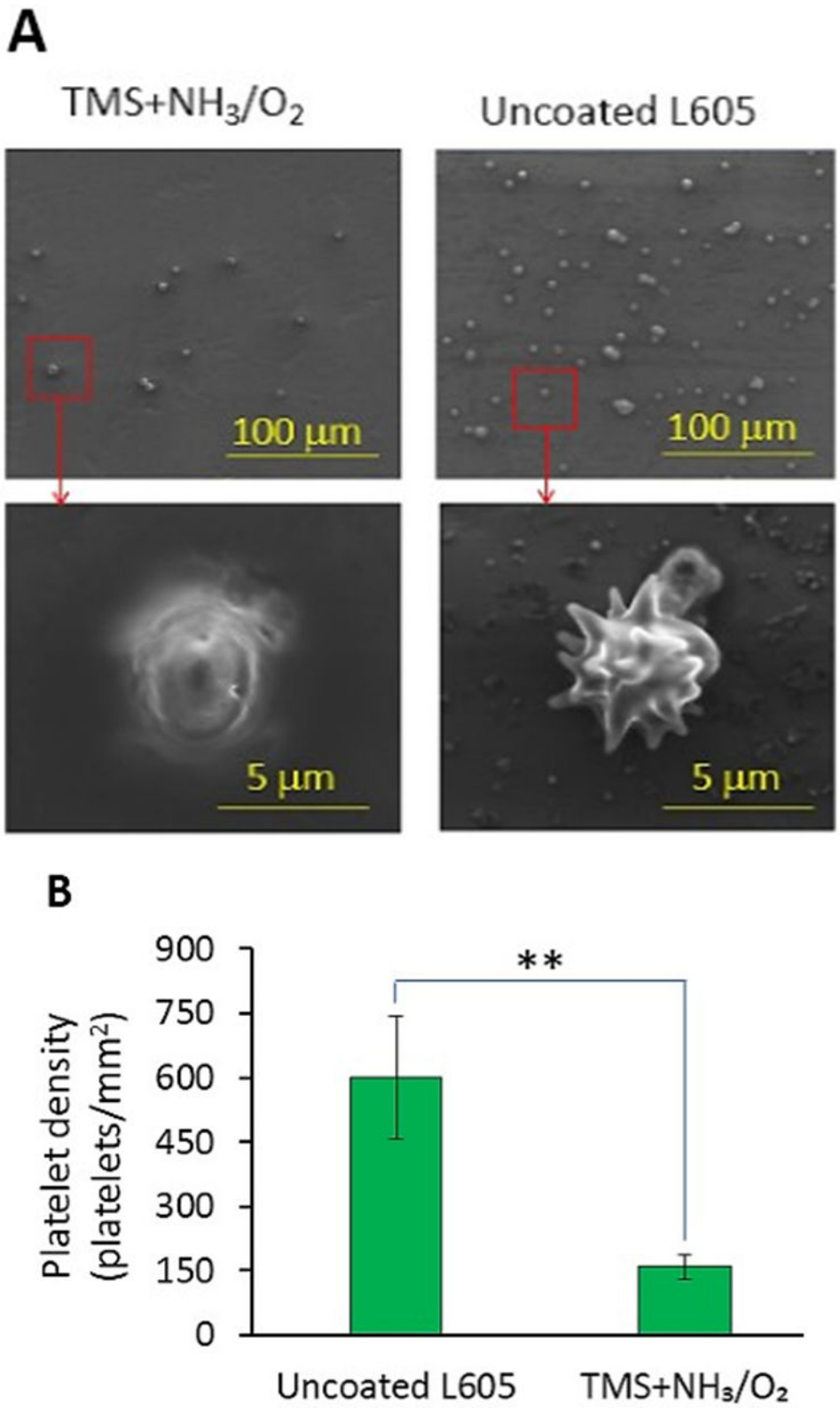

Author Manuscript Author Manuscript Author Manuscript Author Manuscript

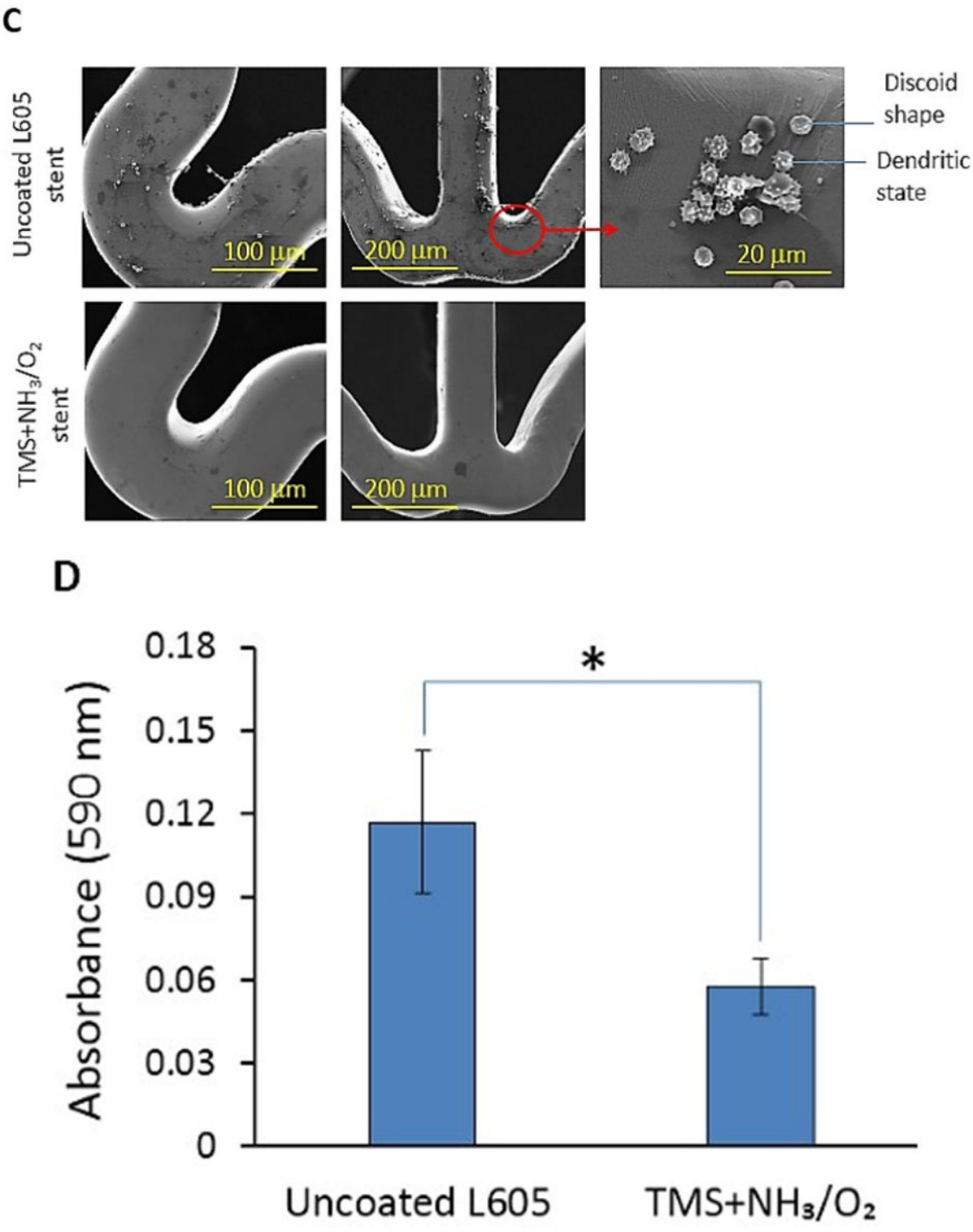

Figure 10:

A) SEM images of platelet adhesion and activation on uncoated L605 and TMS + NH_3/O_2 plasma nanocoated coupons; B) Platelet density on uncoated L605 and TMS + NH_3/O_2 plasma nanocoated coupons, evaluated by ImageJ, indicating values are mean ± SD (n =

Author Manuscript Author Manuscript Author Manuscript Author Manuscript

6), $^{**}p < 0.005$; C) SEM images of platelet adhesion and activation on uncoated L605 and TMS + NH_3/O_2 plasma nanocoated stents; D) Clotting level on uncoated L605 and TMS + NH_3/O_2 plasma nanocoated coupons, determined by absorbance 590 nm. Indicating values are mean ± SD (n = 6), $^{*}p < 0.05$.

Author Manuscript Author Manuscript Author Manuscript Author Manuscript

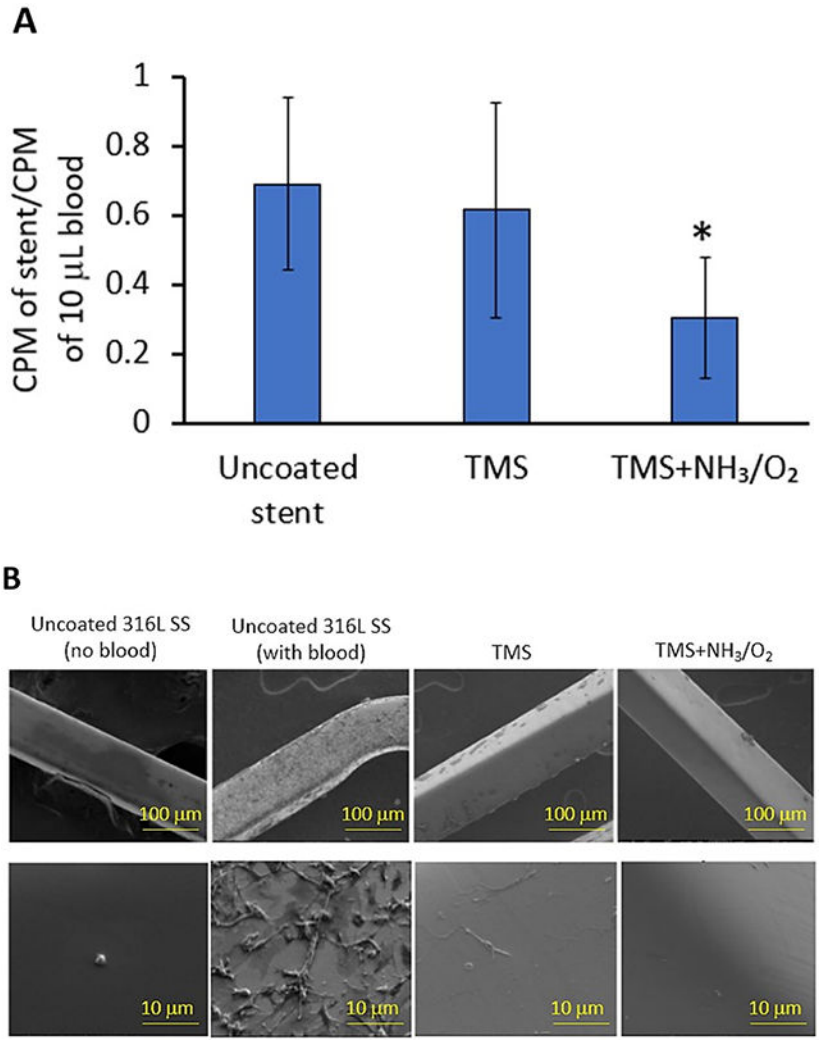

Figure 11:

A) Deposition of indium-111-labeled platelets to uncoated, TMS, and TMS + NH_3/O_2 plasma nanocoated 316L SS stents was assessed in an *ex vivo* perfusion chamber, as described in Methods. Radioactive counts per minute (CPM) of stents retrieved from the perfusion circuit were measured and normalized to radioactive CPM of a sample (10 µL) whole blood perfused within the circuit. Plotted values are means ±SD (n=12). *$p < 0.003$; B) Platelet adhesion to uncoated, TMS, and TMS + NH_3/O_2 plasma nanocoated 316L SS stents was visualized by SEM.

Author Manuscript

Author Manuscript

Author Manuscript

Author Manuscript

Table 1:

Surface elemental composition of TMS plasma nanocoatings with NH_3/O_2 post-treatment.

Element \ Samples	1-day old TMS+NH_3/O_2		Aged TMS+NH_3/O_2 for 2 years	
	Con. (at%)	Ratio to Si2p	Con. (at%)	Ratio to Si2p
O 1s	41.21 ± 1.06	1.292	42.41 ± 1.04	1.413
N 1s	2.77 ± 0.18	0.087	2.6 ± 0.11	0.087
C 1s	24.12 ± 1.70	0.756	24.98 ± 1.5	0.832
Si 2p	31.90 ± 1.08	1	30.01 ± 0.89	1